Negative-kaon and antiproton production near 700 MeV/c by 28.4-GeV/c protons

J. M. Snow,* S. Axelrod, R. L. Morrison, and M. E. Zeller
Yale University, New Haven, Connecticut 06520

D. M. Lazarus
Brookhaven National Laboratory, Upton, New York 11973

H. Nicholson
Mt. Holyoke College, South Hadley, Massachusetts 01075

J. A. Thompson
University of Pittsburgh, Pittsburgh, Pennsylvania 15260
(Received 3 December 1984)

We present measurements of kaon and antiproton production cross sections in the momentum region of 700 MeV/c from 0° to 10° by 28.4-GeV/c protons on complex nuclei. A model to describe the A dependence of these cross sections is discussed and compared with these and other data.

I. INTRODUCTION

In a low-energy separated beam at the Brookhaven Alternating Gradient Synchrotron (AGS),[1] we have measured the production cross sections for kaons and antiprotons in the kinematic region of 700 MeV/c, near 0°, by 28.4-GeV/c protons. Aluminum, copper, and platinum targets were also used to study the dependence of these cross sections on nucleon number.

While low-energy beams have existed for many years and production cross sections from complex nuclei have been measured by many groups, there are scant data in the kinematic region of this experiment. Table I summarizes those which do exist for incident-proton momenta below 30 GeV/c.[2–12]

In addition to the interest in particle-production cross sections for their fundamental physics merit and for future facility development, there is a long-standing discussion about the nucleon-number dependence of particle production mechanisms.[13–20] In this paper we pursue this discussion by presenting a cascade model which employs known particle-particle interaction phenomena to describe production in nuclear matter. The results of this model are compared with our data and that of other experiments over a wide range of incident- and secondary-particle momenta.

We begin by describing the beams and detectors involved in the measurement. This is followed by a description of the data-acquisition and analysis techniques; our cross-section results and comparison with an empirical model; and, finally, the formulation, predictions, and comparisons of our model with published data.

II. PRIMARY BEAM

The primary beam of 28.4 GeV/c protons was extracted from the Brookhaven AGS and transported by the C and C3 beam lines to the production target. Typically this beam had an intensity of $(2–3)\times10^{12}$ protons per machine pulse (approximately 0.9 second in duration), and had a Gaussian profile with full width at half maximum (FWHM) of 8.6 mm horizontally and 3.3 vertically.

TABLE I. Previous negative-kaon-production measurements.

Incident momentum (GeV/c)	Secondary momentum (GeV/c)	Particle	Angular range (mr)	Target	Reference
24.0	4.0–18.0	$K^-,\bar{p}$	17–127	Be,Al,Cu,Pb	2
12.3	0.5–1.0	$K^-,\bar{p}$	0–175	Be,Cu	3
19.2	0.6–1.2	$K^-,\bar{p}$	260	Be	4
18.8, 23.1	4.0–12.0	$K^-,\bar{p}$	0,100	Be	5
12.5	2.9–5.8	K^-	35–140	Be	6
30.0	1.8–2.0	$K^-,\bar{p}$	230	Al	7
10.0–30.0	1.3–16	$K^-,\bar{p}$	83–350	Be,Al	8
12.9	0.7–2.1	$K^-,\bar{p}$	0	Be	9
10.0–24.0	0.4–1.4	$K^-,\bar{p}$	0	C,Cu,W	10
24.0, 26.0	0.6, 1.2	$\bar{p}$	310	Be	11
27.0	0.6–4.1	$\bar{p}$	200	Be	12

These profiles were determined both by means of segmented-wire ion chambers (SWIC's) upstream of the target and by measurement of secondary-beam rates as a function of primary-beam position, this position being controlled by magnets in the C3 line. The latter method of measuring the beam profile was also used to ensure maximum primary beam on the production target.

The absolute number of protons on the target was determined by measuring the total-beam intensity using a secondary-emission chamber (SEC) located 1.64 m upstream of the target, and computing the overlap probability of the beam distribution with the target cross-sectional area. The SEC was calibrated by aluminum-foil-irradiation techniques twice during the experiment. The two measurements agreed to within 10%, and this error is included in the uncertainty estimates of the overall normalization of the cross sections.

The platinum, copper, and aluminum production targets were limited to approximately $\frac{1}{14}$ of a strong-interaction length to minimize tertiary production and secondary interactions by the desired particles. These targets were 0.5 cm high by 1 cm wide and 0.635, 0.914, and 2.29 cm along the primary beam, respectively.

III. SECONDARY BEAM AND DETECTOR

The secondary beam, identified as the C8 beam line at the AGS, is shown in Fig. 1. The proton beam, inclined at an angle of 5° from the optical axis of the C8 line, impinged on the production target at the position designated by the X on the left-hand side of the figure; the X on the right-hand side is the final-image point. The first element is a vertically deflecting dipole ($P1$) followed by a horizontally focusing quadrupole ($Q1$), a 45° sector dipole ($D1$), a sextupole (SEX1), and a vertically focusing quadrupole ($Q2$). These magnets focus rays from the target to a horizontally dispersed image at the sextupole (SEX2) located between the two beam separators (BS1 and BS2). Collimators ($K1$ and $K2$), located upstream and downstream of SEX2, limit the momentum acceptance of the beam. The vertical focus for the $Q1$-$Q2$ doublet occurs downstream of the second beam separator at the vertically collimating "mass slit" (K3). The mass slit is in the entrance of a horizontally focusing quadrupole ($Q3$), followed by a vertically focusing quadrupole ($Q4$), a 45° sector dipole ($D2$), and a horizontally focusing quadrupole

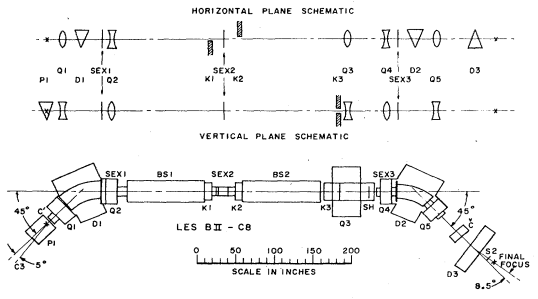

FIG. 1. Diagrams of the C8 beam line showing the functional properties of the optic system in the upper part of the figure and the physical layout of the beam in the lower.

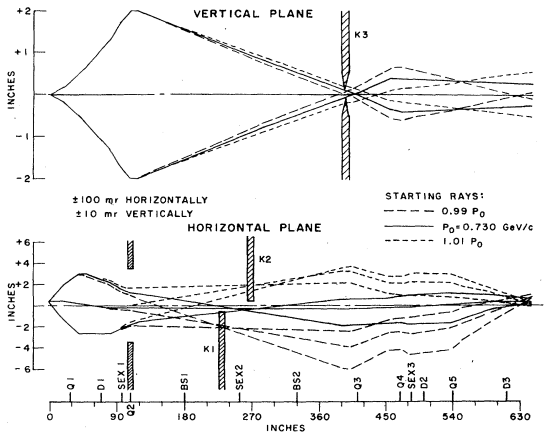

FIG. 2. Ray trace of selected rays transported through the C8 beam. The collimators $K1$ and $K2$ are shown as employed in this experiment.

($Q5$). The beam elements $Q3$ to $Q5$ form an approximate triplet-quadrupole system to focus the intermediate images to a final image in both the horizontal and vertical planes. The dipole $D3$ was a spectrometer magnet used in subsequent experiments.

The solid angle $\Delta\Omega$ and fractional momentum acceptance ΔP were approximately 6 msr and 0.06 (FWHM), respectively. Values of $\Delta\Omega\,\Delta P$ were calculated in detail by Monte Carlo techniques using a modified version of the beam-transport program BETRAF. Sample rays through the apparatus are shown in Fig. 2.

The vertical acceptance of the beam, ±15 mr, was established by the gap of the separator BS1, while the horizontal acceptance of ±100 mr was determined by a collimator in $Q2$. Measurement of the angular dependence of the production cross section near 0° was facilitated by varying the vertical-production angle into this small acceptance with a movable target in the gap of $P1$. The target was positioned, and the current in this magnet adjusted, so that rays with a desired production angle would enter $Q1$ along its optic axis. This procedure is shown schematically in Fig. 3. The full momentum acceptance of the beam with the $K1$ and $K2$ jaws fully open was $\Delta P/P \simeq \pm 0.03$. For this experiment, however, the momentum pass was limited to $\Delta P/P \simeq \pm 0.003$. Figure 2

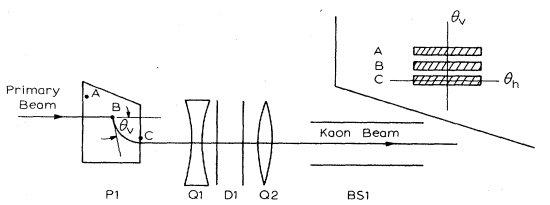

FIG. 3. Schematic diagram of the method of angle selection using the $P1$ pitching magnet. The insert in the upper right shows the acceptance of the beam line in horizontal angle (θ_h)—vertical angle (θ_v) space for different target-position settings (A,B,C).

shows these stops in this configuration while depicting high- and low-momentum rays (±0.01) which are passed if the stops are open.

Located at the exit of the mass slit was a scintillation-counter hodoscope of ten counters, SH_i which determined the horizontal position of rays at that point in the beam. These counters, each 3.18-cm wide and 5.1-cm high, and the position of the target determined the angles of production. Variation in the vertical position of the target resulted in a corresponding variation in the polar production angle of acceptance of a particular SH counter. For the several target positions different counters could subtend the same production angle, thus allowing redundancy in the cross-section measurements.

The detector system included the SH hodoscope, a scintillator $S2$ at the final focus, and a Čerenkov counter $\check{C}$ used to veto pions in the beam. The detectors are shown in Fig. 1. Particle identification was made by measurement of the time of flight of beam particles from the SH counters to $S2$. At the highest beam momentum, 730 MeV/c, the time-of-flight difference between kaons and pions was 3.4 ns and that between antiprotons and kaons was 7.5 ns.

IV. DATA ACQUISITION

At each momentum and target position, magnet currents in the secondary beam line C8 were adjusted. Specifically, $Q1$ and $Q2$ were tuned for maximum transmission through the transport system, and the separator BS1 was set to send the desired particles through the mass slit. In this process $Q2$ was the most sensitive factor since this magnet exercised the greatest control over the longitudinal position of the intermediate vertical focus. As mentioned above, for each change in target position the primary beam C3 was tuned to optimize the number of protons incident on the production target.

Once the beams were turned, data samples were taken with the separators set to transmit separately kaons, antiprotons, and pions. The pion sample established a background time-of-flight spectrum to be subtracted from the kaon and $\bar{p}$ data. A run was also taken with an empty target holder to determine backgrounds not associated with the target. Typically, empty backgrounds were less than 10% of the signal levels and were appropriately subtracted in the data-reduction process. As a further check on the measurement, data were taken with two openings of the mass slit.

The data consisted of the SH_i counter hit information, and the $SH_i \cdot S2$ time of flight for each event; scaler information for SH, $S2$, $SH \cdot S2 \cdot C$ for each machine pulse; and monitor information from the SEC. Also the proton flux in the C line was noted for each data run. From the scaler information and the time-of-flight spectra the number of kaons or antiprotons observed at the exit of the secondary beam per proton in the incident beam was extracted.

V. DATA ANALYSIS

The doubly differential cross section in the laboratory frame for the ith SH counter in units of square centimeters per steradian per GeV/c per nucleus is calculated from the equation:

$$\frac{d^2\sigma_i(\theta_i,P)}{d\Omega\, dP} = \frac{n_i k A}{\Delta\Omega_i \Delta P_i x N_a \rho T_P h (1-f)(1-g)}, \quad (1)$$

where θ_i = the average production angle accepted in the ith SH counter (mr), P = the average momentum in the beam acceptance (GeV/c); $\Delta\Omega_i$ = accepted solid angle in the ith SH counter (sr), ΔP_i = accepted momentum range of the ith SH counter (GeV/c), n_i = counts in the ith SH counter after background subtraction, k = decay-in-flight factor, A = atomic weight of target nucleus (g), x = target length (cm), N_a = Avogadro's number, ρ = density of the target (g/cm^3), T_P = integrated number of protons at the target, h = fraction of incident protons on the target, f = average fraction of protons absorbed in the target, g = fraction of secondaries absorbed by beam-line material.

The factors θ_i, $\Delta\Omega_i$, ΔP_i, and P were determined from the Monte Carlo beam-ray-tracing program. This was accomplished by generating particle trajectories uniformly over a 4π solid angle and broad momentum band, and averaging the production angles and momenta of those rays accepted in the ith SH counter. Absorption of the secondary particles in the target was also included at this point.

The experimental number of counts in the ith SH counter, n_i, was determined from the time-of-flight spectra after subtraction of normalized pion and empty target spectra, with the time distribution of pions being determined from runs with the separators tuned to pions. Raw data and subtracted spectra are shown in Figs. 4 and 5 for kaons and antiprotons, respectively. The subtraction procedure was followed for each SH counter in each data run. The number of particles detected in each counter was then determined by summing the total number of counts in the respective distribution.

Fractional absorption of primary and secondary particles, f and g, were calculated using known absorption cross sections and were typically $f \simeq 0.033$ for protons, $g \simeq 0.017$ for kaons, and $g \simeq 0.075$ for antiprotons. The factor due to decay in flight, k, including the probability that decay products can remain in the signal sample, is set equal to one for antiprotons and 19.7, 27.0, and 36.7 for kaons with average momenta of 0.730, 0.662, and 0.606 GeV/c, respectively.

The statistical uncertainty in the subtracted signal ranges from about 2% of the signal for the most populated counters to 20% of the signal for the counters at the periphery of the acceptance. An 11% uncertainty in the signal arises from uncertainty in the SEC calibration and in the estimate of fraction of beam on target.

The ability to measure cross sections at the same kinetic points with different target settings, as well as the ability to measure cross sections at different angles simultaneously with the various SH counters, allowed checks on the measurements. The counter populations were simulated by the Monte Carlo calculation for the several data-acquisition configurations. The solid angle of the beam system was thus determined using the known properties of

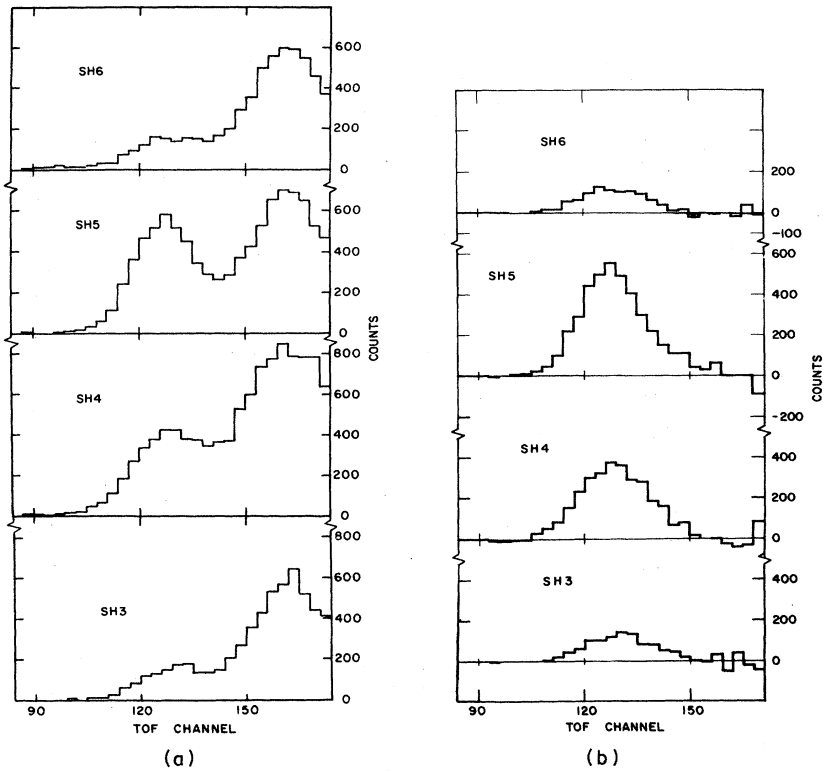

FIG. 4. Time-of-flight (TOF) spectra for kaon data for SH counters 3 through 6. High channels correspond to early times; calibration is approximately 10 channels/ns. (a) Raw spectra, (b) spectra with pion time-of-flight distribution subtracted.

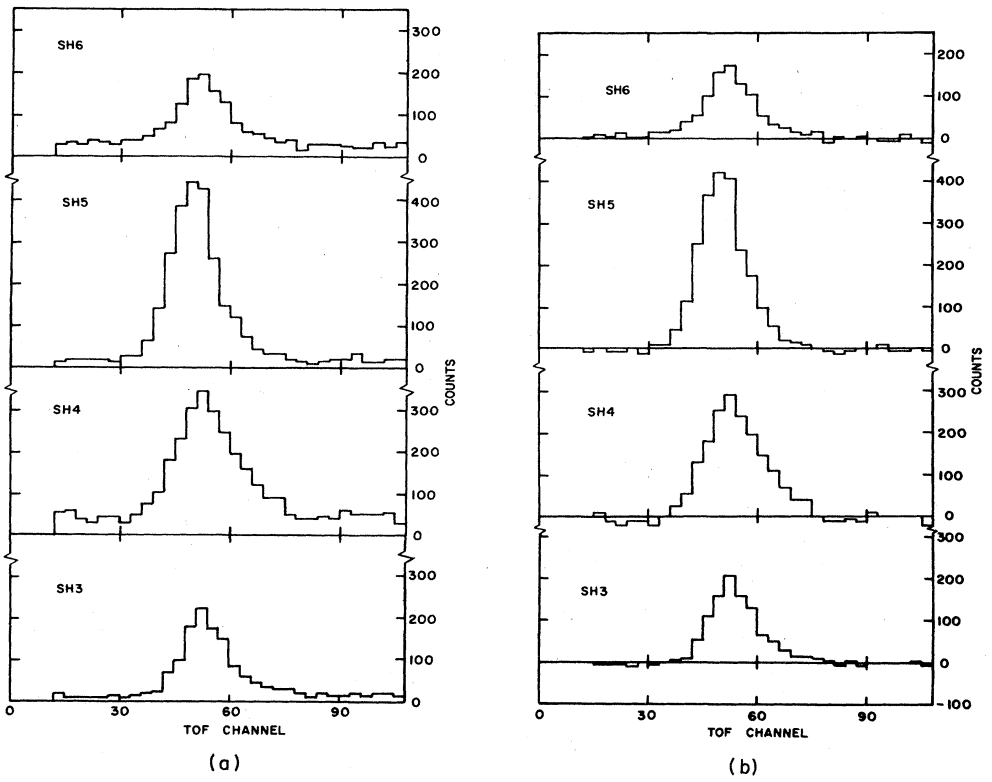

FIG. 5. Time-of-flight spectra for antiproton data. (a) Raw spectra, (b) pion-subtracted spectra.

TABLE II. Differential cross sections for K^- production by 28.4-GeV/c protons.

Momentum (GeV/c)	Material	Angle (deg)	$d^2/\sigma/d\Omega\, dP$ [mb/(sr GeV/c)]
0.730	Pt	3.07	19.61±1.62
		5.04	22.59±2.26
		7.39	15.61±1.16
		8.53	10.50±1.09
0.730	Cu	2.76	7.68±0.66
		5.33	6.09±0.50
		7.48	5.00±0.43
		9.41	3.52±0.68
0.730	Al	3.04	3.48±0.35
		4.51	3.06±0.38
		7.04	2.53±0.27
		8.61	2.66±0.59
0.660	Pt	2.83	23.75±1.67
		4.29	20.27±1.45
		6.80	15.12±2.34
		8.58	12.05±0.79
		10.46	12.30±2.06
0.660	Pt	3.17	18.36±3.07
		4.36	17.09±1.85
		8.92	9.93±0.85
		10.95	7.89±1.33

the beam-transport elements. By varying the parameters of the beam elements within their known tolerances and generating new SH counter distributions for the altered parameters, the same program determined the uncertainties in the solid angles. A constraint in this process was that the generated counter distributions be consistent with the observed distributions.

VI. KAON CROSS SECTIONS

The results of the kaon-production measurement are given in Table II and depicted in Fig. 6. Since the production cross sections from platinum vary only slightly over our momentum range, the results for all momenta can be shown in the same figure. Also shown are the results for copper and aluminum at 730 MeV/c. The straight lines in this figure are the results of the least-square fits to the 730-MeV/c points. Extrapolating these lines to 0°, we show in Fig. 7 the 0° cross sections as a function of target nucleon number with a straight-line fit to the data superimposed on the double-logarithmic plot. The parameters of that fit are given in the figure. The resultant exponent for the A dependence is 0.867±0.064.

Figure 8 presents all of the data at 730 MeV/c divided by their respective values of $A^{0.867}$. As can be seen, the angular dependence of the cross section is not affected by the different materials. To put these data into the context of what might be expected we present in Fig. 8 three curves based on parametrization of Sanford and Wang.[21] This parametrization is the result of an empirical formula which gives a representation of secondary-particle production over all angles up to 30° and secondary momenta up to 26 GeV/c in proton-beryllium collisions. The curve marked A is the direct result of this parametrization and

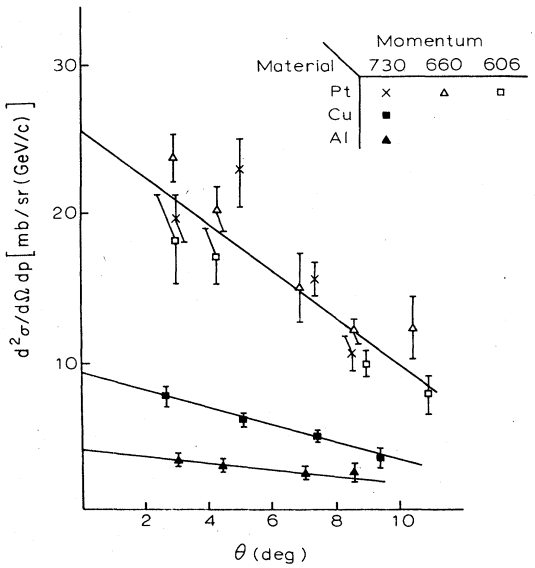

FIG. 6. Kaon-production cross sections for different targets and momenta as labeled by the symbol table in the upper right-hand corner of the figure.

shows structure which is inconsistent with our data. When the fit was made in 1967, there were no data near 0° and low secondary-particle momenta. Since this prediction was thus made from data taken at higher momenta and larger angles, the inconsistency with our results is not surprising.

By the method of kinematic reflection[22] one can use the high-momentum region to synthesize the low. This is a more reliable technique insofar as the parametrization was made with the high-momentum data. It has some limitations, however, both because of neutrons in the target ma-

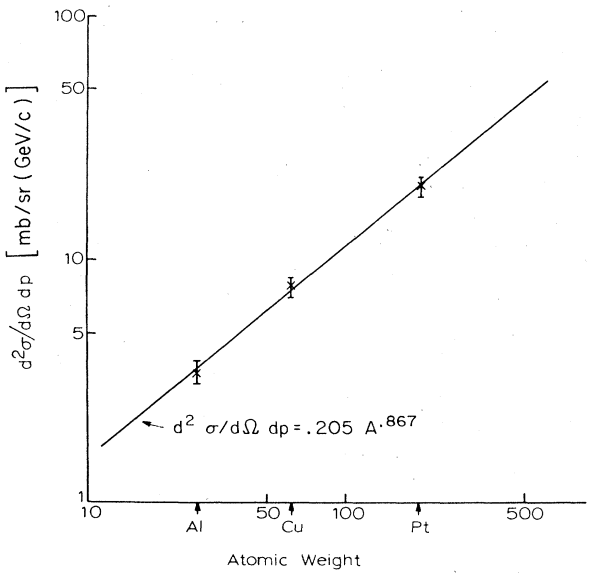

FIG. 7. 0° extrapolations of kaon-production cross sections at 730 MeV/c as a function of atomic weight. The straight line is the result of a fit to the data with parameters as shown.

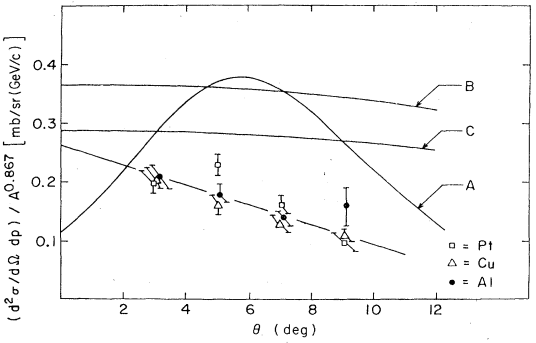

FIG. 8. Kaon-production data at 730 MeV/c divided by $A^{0.867}$. The line through the data points is meant to guide the eye; curve A is a direct calculation of Ref. 21 divided by 4; curve B is a kinematically reflected calculation of Ref. 21; curve C is kinematically reflected data from Ref. 2 as described in the text.

terial, and differences between high- and low-momentum interactions in the nuclear matter of the target. Curve B in Fig. 8 is a result of kinematic reflection applied to the Sanford-Wang parametrization (SWKR).

When the original formulation was constructed in 1967, the forward production data which applies to our kinematic region was also limited. Since then a much larger sample has been collected, and we present results employing the new data in curve C of Fig. 8. These data were gathered by Eichten *et al.*[2] at 24-GeV/c incident-proton momentum with secondary momenta of 4 GeV/c and above, and at angles of 17 mr and above. We have used their beryllium data, scaled it for projectile momentum from 24 GeV/c to 28.4 GeV/c according to the prescription of Sanford and Wang, applied kinematic reflection, and scaled the result in atomic number by $A^{0.867}$ to obtain curve C (EKR). While not achieving consistency over the entire angular range, this new formulation is in agreement with the data near 0°, and is a definite improvement over the other attempts.

TABLE III. Differential cross sections for $\bar{p}$ production by 28.4-GeV/c protons from platinum.

Momentum (GeV/c)	Angle (deg)	$d^2\sigma/d\Omega\,dP$ [mb/(sr GeV/c)]
0.730	3.60	0.118±0.019
	4.41	0.117±0.041
	6.76	0.132±0.033
	8.24	0.102±0.011
	10.09	0.086±0.017
0.660	3.55	0.104±0.013
	7.13	0.112±0.028
	8.58	0.060±0.006
	10.39	0.050±0.010
0.606	3.56	0.046±0.040
	4.28	0.061±0.009
	6.85	0.032±0.007
	9.37	0.049±0.007
	10.75	0.023±0.006

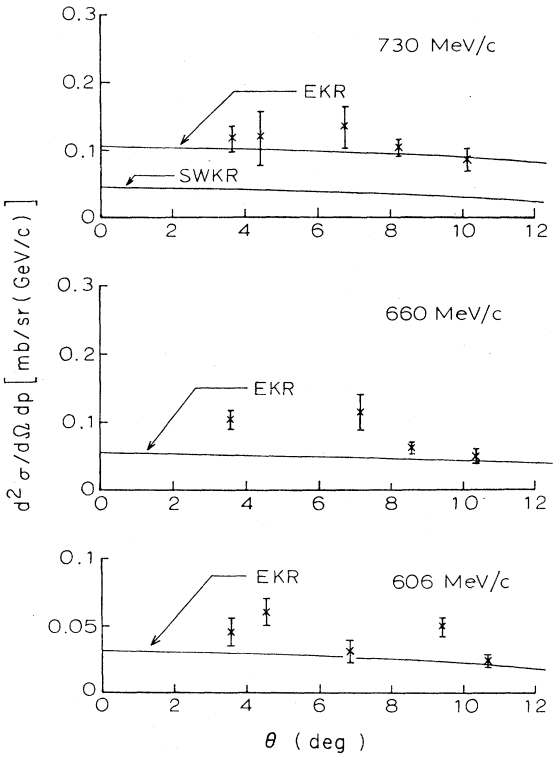

FIG. 9. Antiproton-production cross sections from platinum at 730, 660, and 606 MeV/c. The curves labeled SWKR and EKR are described in the text.

VII. ANTIPROTON CROSS SECTIONS

Tabulated in Table III and shown in Fig. 9 are the antiproton cross sections from platinum at 730, 660, and 606 MeV/c; platinum being the only material used for $\bar{p}$ production. Also shown in the figure are the SWKR and EKR fits. Again, since the available data in 1967 when the Sanford-Wang formulation was made were limited, the lack of agreement between our data and SWKR is not surprising. The EKR curves do fit our data fairly well.

In computing the fits shown in Fig. 9 we have scaled the beryllium data of Ref. 2 and the Sanford-Wang predictions by $A^{0.77}$ in contrast to the kaon scaling of $A^{0.867}$. The motivation for this is the result of the model prediction described below.

VIII. A MODEL FOR THE A DEPENDENCE OF PRODUCTION CROSS SECTIONS

Particle-production cross sections from complex nuclei seem to have a dependence on nucleon number A of the form $A^{\alpha(x)}$, where x is the Feynman scaling variable. (For complex nuclear targets $x = P_{||}/P_{\max}$ evaluated in the Lorentz frame in which the projectile and target nucleons have equal and opposite momenta.) As noted by Barton *et al.*,[19] for $x > 0.1$ a curve of functional form

$\alpha(x)=0.74-0.55x+0.26x^2$ fits the bulk of the data for proton production of various secondary particles with incident-proton momenta ranging from 24 to 300 GeV/c; the noted exceptions for $\bar{p}$ and Ξ^0 production. This is, of course, contrary to the expected exponent of $\frac{2}{3}$ for a strongly screened nucleus. This phenomenon has been speculated upon for forward particle production, but no models which included the full range of x have been developed.

In an attempt to understand how the A dependence of our data might be related to those in other kinematic regions, we investigated a rather simple cascade model. A complete cascade calculation would require a simulation of all of the processes which occur in nucleon-nucleon and meson-nucleon interactions as the projectile and secondary particles pass through the matter of the target nucleus. Such a simulation would be based on known particle-particle interaction cross sections, and might be made with Monte Carlo techniques or by convoluting and permuting probability functions of the various processes. Since our interest was in understanding $\alpha(x)$, which involves the ratio of production from heavy and light nuclei, a greatly simplified calculation could be pursued. We outline this calculation and give its results below, and present a more detailed description in the Appendix.

Consider a projectile penetrating a distance y into a nucleus and producing the desired secondary particle at y within a small region dy. The basis of our formulation is that the projectile, when found traversing such a distance within nuclear matter, has a probability of losing energy from strong interactions while not losing its identity. This is the well-known leading-particle effect as most explicitly seen in pp and πp inclusive reactions.[23] In addition, there is the probability of a loss of the projectile once it has interacted in the distance y, as well as the probability that the projectile will not interact at all. If the projectile is not absorbed but interacts, it arrives at y with momentum $P=x_p\ P_{\rm inc}$, where $P_{\rm inc}$ is the incident momentum and x_p is the Feynman x, chosen with the weighting of a fragmentation function $\bar{f}(x_p,P)$,[23] (P is zero for forward production). In the case of no interactions x_p is equal to 1. The secondary particle is produced within dy from an appropriate distribution, in this case the parametrization of Sanford and Wang, with a momentum P_K'. It then proceeds through the remainder of the nucleus: losing momentum in the same manner as the projectile and emerging with momentum P_k, being absorbed, or not interacting at all. In the latter case the secondary particle is produced with its final momentum. We have used the same fragmentation function in the energy loss of the secondary particle as that of the projectile.

The fragmentation function which we have used from which to choose the fraction of momentum retained by a particle after interacting is derived from the invariant cross section for particle-nucleon scattering:

$$\frac{d\bar{f}}{dx}(x,P)=\frac{N}{x}E\frac{d^3\sigma}{dP^3}dP^2\ . \tag{2}$$

Here E and P refer to the energy and momentum of the scattered particle, and N is a normalization factor to constrain $\int_0^1(d\bar{f}/dx)dx=1$. The invariant differential cross section is that for $pp\rightarrow pX$.

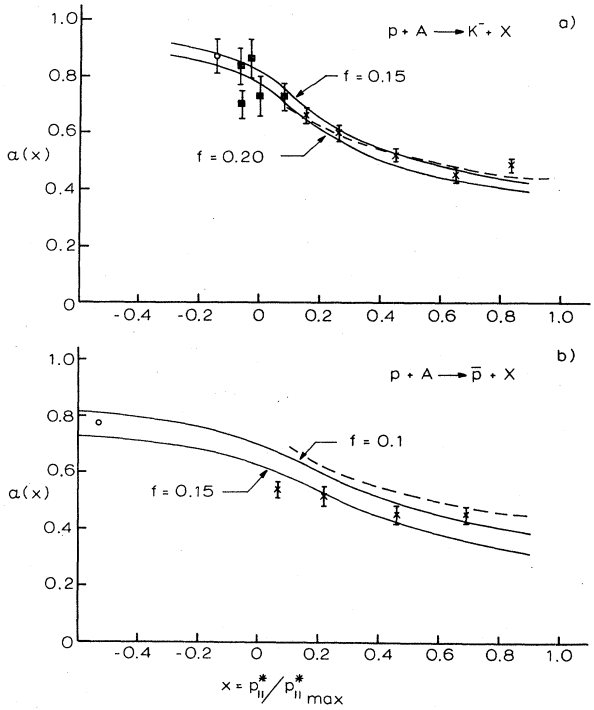

FIG. 10. The exponent $\alpha(x)$ as a function of Feynman x for kaon production (a) and antiproton production (b). Symbols are as follows. ×, Ref. 2; solid squares, Ref. 10. The circle is the value used to derive the EKR curves of Fig. 9. The solid curves are the results of the model described in the text, the dashed curves are the formulation of Ref. 20.

In order to describe the probability that the projectile or secondary particle might be lost from the system, either by scattering out or by losing its identity upon interacting, we introduce a free parameter f. In the interaction probability function this parameter multiplies the total absorption cross section for the particular particle incident on protons. It can thus be interpreted as the fraction of the absorption cross section responsible for the loss of the particle.

The result of the calculation is the variation of α as a function of x of the secondary particle, and is depicted for kaons and antiprotons in Fig. 10. The data shown in the figure are those of this experiment as well as those of Refs. 2 and 10. We display curves for two values of f which yield reasonable fits to the data to demonstrate the sensitivity of the predictions to this parameter. The dashed curve is the functional form of Ref. 20. We find it interesting that the values of f which yield reasonable fits are physically sensible, i.e., about 15% of the absorption cross section causes particles to be lost from the system.

That there is only small dependence of $\alpha(x)$ on the energy is built into the model by making the energy-loss mechanism dependent on Feynman scaling rather than energy, as is observed in pp inclusive reactions. Thus, while the final particle-production spectrum is strongly dependent on the particle-generating function, the ratio of production at a given x for different nucleon numbers is less

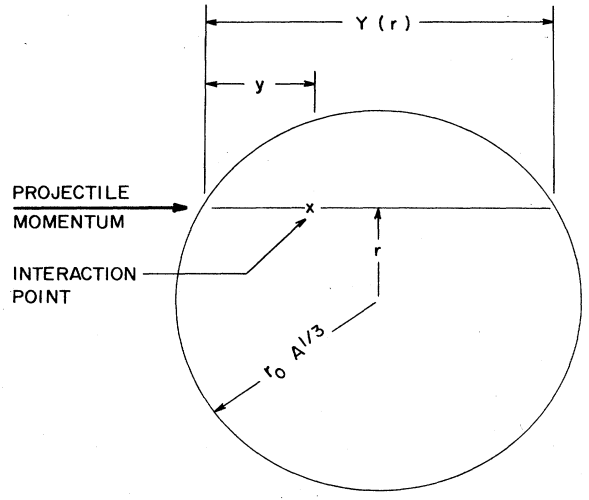

FIG. 11. A schematic drawing of a complex nucleus with an incident projectile impinging from the left at a distance r from the center of the nucleus and interacting at y within dy.

so. For example, the Sanford-Wang formulation was originally made for 30 GeV and below, but for kaon production at 100 GeV incident-proton momentum we obtain an $\alpha(x)$ distribution which is essentially the same as that shown in Fig. 11. The calculated kaon spectrum, however, drops off significantly faster with increasing x than that observed experimentally.

We have also investigated tertiary-kaon production via pion-nucleon interactions where the pions were produced in primary proton-nucleon collisions. These yields were negligibly small compared to kaon production from protons, and have not been included in our determination of α. This is not a surprising result since kaon-production cross sections are approximately proportional to $P_{\rm inc}{}^{-1/2}$, where $P_{\rm inc}$ is the incident momentum of the particle producing the kaon,[21] and pions are produced preferentially with low Feynman x, i.e., with a small fraction of the incident proton momentum.

In Fig. 10(b) one sees that the antiproton data do indeed disagree with the fit of Barton *et al.*[20] to previous data, but are better described by our model. The difference between the kaon and antiproton curves arises from the difference between their respective interaction cross sections.

In scaling kinematically reflected published $\bar{p}$ production data from beryllium[2] to our data from platinum, we have used the value of $\alpha=0.77$ at $x=-0.53$ as determined by our calculation, the circle in Fig. 10(b). The curves labeled EKR in Fig. 9 are the results of this scaling and, considering that they are derived from data for forward production from beryllium at incident-proton energy of 24 GeV, they represent our data fairly well.

Many of the publications which speculate on the nature of particle production from complex nuclei do so from the point of view of quark models.[15–19] This is not at odds with our model since the underlying mechanisms which produce leading-particle effects are indeed a result of quark interactions. In contrast to those models, however, we do describe $\alpha(x)$ in the target fragmentation region in a consistent way, with minimal input from published production data. The structure of our model (projectile-energy loss, secondary-particle production, and subsequent energy loss) is more that of an additive quark model than a constituent quark model. In the latter case constituent quarks from the projectile interact coherently with the nucleus, fragment, and are recombined in a manner independent of the fact that the collision took place in nuclear matter. In the additive quark model the constituents of the projectile interact incoherently with those of the target yielding "wounded" quarks and spectators which then become hadrons. A difference between our model and the quark models, however, is that ours involves the probability of multiple interactions within nuclear matter of both the projectile and the secondary hadron. The quark models consider only single interactions.

IX. CONCLUSION

We have presented production cross sections for kaons and antiprotons in a new kinematic region. These results will be of value if new kaon factories are constructed since low-momentum kaon beams will be important for these facilities. In an attempt to understand these cross sections we have constructed a model of the A dependence of the production which successfully describes data over a wide kinematic range for both kaon and antiproton production.

ACKNOWLEDGMENTS

We are most grateful for the assistance of L. Trudell in constructing the apparatus, and to T. Kycia for loaning us the Čerenkov counter. We also thank the staff of the AGS, and especially M. Iarocci for their support in assembling and executing this experiment. This research was supported in part by the Department of Energy under Contracts Nos. (Yale) DE-AC02-76ER03075 and (BNL) DE-AC02-76CH00016.

APPENDIX

We present in this Appendix details of the computational process involved in calculating $\alpha(x)$. We begin by depicting the path of the projectile through a spherical nucleus, see Fig. 11. The path passes a perpendicular distance r from the center of the nucleus and has a total length $Y(r)$ through the nucleus. The radius of the nucleus is $r_0 A^{1/3}$ and the particular interaction point which we consider is at y within dy.

We now define the following functions:

R_1 is the probability that the projectile reaches y without interacting,

$$R_1 = e^{-\rho y \sigma_P} ; \tag{A1}$$

ρ is the nuclear matter density and σ_P is the total interaction cross section per nucleon of the projectile. The momentum of the projectile producing the secondary particle is $P_p = P_{\rm inc}$.

R_2 is the probability that the projectile reaches y after interacting and retains its identity,

TABLE IV. Model parameters.

Parameter	Symbol	Value
Nuclear density	ρ	0.15 nucleons/fm^3
Proton interaction cross section	σ_p	31 mb
Kaon interaction cross section	σ_k	20 mb
Antiproton interaction cross section P=antiproton momentum in GeV/c	σ_k	$(40+33/\sqrt{P})$ mb
Nucleon radius	r_0	1.26 fm
Fragmentation function:		
$\bar{x}$	Δx	$d\bar{f}/dx$
0.25	0.35	0.75
0.45	0.20	1.15
0.65	0.20	1.09
0.82	0.15	1.04
0.95	0.10	1.46

$$R_2=(1-e^{-\rho y\sigma_P})(1-e^{-f\rho y\sigma_P}) . \quad \text{(A2)}$$

The momentum of the projectile is $P_p=x_pP_{\text{inc}}$.

$R_3(x_P)$ is the probability of the occurrence of x_p given by the fragmentation function $d\bar{f}(x_p)/dx_p$. The normalization of this function is

$$\sum_{x_p=0}^{1}[d\bar{f}(x_p)/dx_p]\Delta x_p=1 . \quad \text{(A3)}$$

R_4 is the particle-production distribution $dN(P_p,P'_K)/dP'_K d\Omega$, in our case the Sanford-Wang distribution. P'_K is the momentum of the secondary particle at production and is related to the final secondary-particle momentum P_K by $P_K=x_KP'_K$.

$R_5(x_K)$ is the probability of the occurrence of x_K given by the above fragmentation function, $d\bar{f}(x_K)/dx_K$.

R_6 is the probability that the secondary particle traverses the distance $[Y(r)-y]$ without interacting,

$$R_6=e^{-\rho[Y(r)-y]\sigma_K} , \quad \text{(A4)}$$

σ_K is the total interaction cross section per nucleon of the secondary particle; for this case $P_K=P'_K$.

R_7 is the probability that the secondary particle interacts but retains its identity after traversing the distance $[Y(r)-y]$,

$$R_7=(1-e^{-\rho[Y(r)-y]\sigma_K})(1-e^{-f\rho[Y(r)-y]\sigma_K}) . \quad \text{(A5)}$$

The contribution to the production of secondary particles of momentum P_K from this interaction region is then given schematically by

$$dN(P_{\text{inc}},P_K,y)=R_1\left[R_4R_6+\left[\sum_{x_K}R_4R_5(x_K)\right]R_7\right]+R_2\sum_{x_P}R_3(x_p)\left[R_4R_6+\left[\sum_{x_K}R_4R_5(x_K)\right]R_7\right] . \quad \text{(A6)}$$

Summation is then made over all values of y from zero to $Y(r)$. This is then weighted by r and summation is made over r from zero to $r_0A^{1/3}$. The probability of loss, of either the projectile or the secondary particle is introduced via the free parameter f. Such a loss occurs if the particle changes its identity or scatters out of the system via a strong interaction. The parameter $\alpha(x)$ is determined by taking the ratio of production from a heavy nucleus such as Pt to that from a light nucleus such as Al. The various parameters used in the model are given in Table IV.

*Present address: Physics Department, University of Oklahoma, Norman, OK 73019.

[1]D. M. Lazarus, in *Proceedings of the Summer Study Meeting on Kaon Physics and Facilities* (Report No. BNL 50579, 1976), p. 119.

[2]T. Eichten *et al.*, Nucl. Phys. **B44**, 333 (1972).

[3]G. J. Marmer *et al.*, Phys. Rev. **179**, 1294 (1969).

[4]J. Duboc, A. G. Minten, and S. G. Wojcicki, CERN Technical Report No. 65-2, 1965 (unpublished).

[5]D. Dekkers *et al.*, Phys. Rev. **137**, 962 (1965).

[6]R. A. Lundy, T. B. Novey, D. D. Yovanovitch, and V. L. Telegdi, Phys. Rev. Lett. **14**, 504 (1966).

[7]V. L. Fitch, S. L. Meyer, and P. A. Piroue, Phys. Rev. **126**, 1849 (1962).

[8]W. F. Baker *et al.*, Phys. Rev. Lett. **7**, 101 (1961).

[9]A. Yamamoto *et al.*, KEK Technical Report No. BM-81-1, 1981 (unpublished).

[10]J. F. Amann *et al.*, LANL Technical Report No. LA9486-MS, UC-34c, 1982 (unpublished).

[11]P. I. P. Kalmus *et al.*, CERN Technical Report No. 71-25, 1971 (unpublished).

[12]U. Amaldi *et al.*, Nuovo Cimento **30**, 973 (1963).

[13]K. Heller *et al.*, Phys. Rev. D **16**, 2737 (1977).

[14]P. Skubic *et al.*, Phys. Rev. D **18**, 3115 (1978).

[15]N. Nikolaev and S. Poxorski, Phys. Lett. **80B**, 290 (1979).
[16]A. Białas and E. Białas, Phys. Rev. D **20**, 2854 (1979).
[17]A. Dar and F. Takagi, Phys. Rev. Lett. **44**, 768 (1980).
[18]G. Berlad, A. Dar, and G. Eilam, Phys. Rev. D **22**, 1547 (1980).
[19]F. Takagi, Phys. Rev. D **27**, 1461 (1983).
[20]D. S. Barton *et al.*, Phys. Rev. D **27**, 2580 (1983).
[21]J. R. Sanford and C. L. Wang, AGS Internal Report No. BNL 11479, 1967 (unpublished).
[22]The method of kinematic reflection relies on the symmetry of *pp* interactions to employ the cross sections for high-energy secondary-particle production (forward-angle production in the center of mass) to calculate low-energy production (backward-angle production in the center of mass).
[23]M. L. Perl, *High Energy Hadron Physics* (Wiley, New York, 1974), pp. 190.